DOI: 10.1002/ejic.201100077

Silver(II) Fluorosulfate: A Thermally Fragile Ferromagnetic Derivative of Divalent Silver in an Oxa-Ligand Environment

Przemysław J. Malinowski,[a] Mariana Derzsi,[b] Zoran Mazej,[c] Zvonko Jagličić,[d] Piotr J. Leszczyński,[b] Tomasz Michałowski,[a] and Wojciech Grochala*[a,b]

Keywords: Silver / Oxidation / Density functional calculations / Fluorosulfate

Several synthetic pathways and characterization of silver(II) fluorosulfate are reported. The title compound crystallizes in the monoclinic space group, $P2_1/c$, with a = 10.5130(4) Å, b = 7.7524(3) Å, c = 8.9366(4) Å, β = 117.867(2)° [V = 643.88(5) Å^3, Z = 4, $d_{calcd.}$ = 3.15 g cm^{-3}] in a structure type related to that of AgF_2. Puckered [$Ag(SO_3F)_2$] sheets are present in the crystal structure with two oxygen atoms of the fluorosulfate anions utilized for bonding within the sheet; the third oxygen atom serves as a linker to the adjacent sheet. Terminal fluorine atoms form small cavities in the structure. The S–O stretching region of the vibrational (IR and Raman) spectra is rich in bands, thus confirming the structural complexity of $Ag(SO_3F)_2$. $Ag(SO_3F)_2$ is a soft ferromagnet with a Curie temperature of 24.8 K and it shows a single broad electron spin resonance (ESR) with g = 2.183 at T = 293 K. The intrasheet magnetic superexchange constant, J, derived from magnetization measurements, equals +1.0 meV per formula unit. Density functional theory calculations suggest that the superexchange occurs through the OO moiety of the Ag–O–S–O–Ag bridge while omitting the S atom, and the yield is J = +1.1 meV. The Coulomb-corrected local spin density approximation (LSDA+U) calculations predict a direct electronic band gap at the Fermi level of 1.05 eV. Large magnetic moments reside on O atoms attached to Ag^{II}; in consequence, $Ag(SO_3F)_2$ is thermally unstable; at room temperature or in the presence of strong acids its dark brown crystals slowly decompose at the surface to a black mixed-valence $Ag_3(SO_3F)_4$. Very fast exothermic decomposition of $Ag(SO_3F)_2$ with emission of a fluorosulfuryl radical ($SO_3F^{\cdot}$) occurs above 120 °C as confirmed by simultaneous thermogravimetric, calorimetric and evolved gas analyses.

Introduction

Fluorides constitute by far and away the majority of inorganic compounds of divalent silver.[1] Although Ag^{II} is a strong oxidant ($E^0[Ag^{II}/Ag^{I}]$ = +1.98 V vs. NHE[2]), it cannot compete in oxidizing power with fluorine ($E^0[F_2/2F^-]$ = +3.05 V vs. NHE[2]), hence the majority of the fluorides of Ag^{II} are thermally stable to several hundred degrees centigrade. However, the corresponding redox potential of the oxide/peroxide redox pair ($E^0[H_2O_2, 2H^+/2H_2O]$ = +1.76 V vs. NHE) is less positive than that of the Ag^{II}/Ag^{I} pair, which places oxygen-based connections of Ag^{II} at the verge of thermodynamic stability at ambient (p, T) conditions. Indeed, theoretical DFT calculations predict that Ag^{II} is capable of transferring the hole from its $4d^9$ set to the 2p band of oxygen in many pseudobinary inorganic connections in the gas phase.[3] Nevertheless, several thermodynamically metastable derivatives of Ag^{II} in the solid state with oxygen in the first coordination sphere of a metal have been reported, notably $Ag^{II}[Ag^{III}O_2]_2$,[4] $Ag^{II}(SO_3F)_2$,[5] $Ag^{II}(SO_3CF_3)_2$,[6] $AgSO_4$[7] and $Ag^{II}(pz)_2(S_2O_8)$, in which pz = pyrazine.[8]

The electronic and magnetic properties of oxa derivatives of Ag^{II} are often surprising due to substantial 4d(Ag)–2p(O) orbital mixing, which vastly exceeds the one seen for analogous Cu^{II} oxide derivatives. In consequence, $Ag^{II}[Ag^{III}O_2]_2$ is supposedly metallic[4] whereas $AgSO_4$ shows an unusually strong antiferromagnetic (AFM) coupling, which persists up to the temperature of thermal decomposition of this compound.[7] The remaining $Ag^{II}(SO_3F)_2$[5] and $Ag^{II}(SO_3CF_3)_2$[6] were only partially characterized in the previous literature reports: (i) limited data is available on the positions of IR bands; (ii) the value of the Curie temperature for ferromagnetic $Ag^{II}(SO_3F)_2$ was initially given as 20 K[5] but was then inconsistently reported as 40 K elsewhere.[9] Crystal structures and other important properties of this compound were not studied.

[a] Faculty of Chemistry, University of Warsaw,
Pasteur 1, 02093 Warsaw, Poland
Fax: +48-22-5540801
E-mail: wg22@cornell.edu
[b] Interdisciplinary Center for Mathematical and Computational Modeling, University of Warsaw,
Pawinskiego 5a, 02106 Warsaw, Poland
[c] Department of Inorganic Chemistry and Technology, Jožef Stefan Institute,
Jamova 39, 1000 Ljubljana, Slovenia
[d] University of Ljubljana, Faculty of Civil and Geodetic Engineering, and Institute of Mathematics, Physics and Mechanics,
Jadranska 19, 1000 Ljubljana, Slovenia
Supporting information for this article is available on the WWW under http://dx.doi.org/10.1002/ejic.201100077.

Due to the paucity of Ag^{II} complexes as well as to extend our previous work on compounds of silver(II) with oxa ligands,[7,10] we explored various synthetic pathways and thoroughly characterized the chemical reactivity and physical properties of pseudobinary fluorosulfate and triflate derivatives of Ag^{II}. In the current work we report the crystal structure of $Ag^{II}(SO_3F)_2$, full vibrational (IR and Raman) and electron spin resonance (ESR) spectra, characterize its magnetic and thermal properties and interpret our findings with the help of periodic DFT calculations. In a parallel report we describe related mixed-valent $Ag_3(SO_3F)_4$.[11] A contribution on related $Ag^{II}(SO_3CF_3)_2$ will follow shortly.[12]

Results and Discussion

Synthesis

The first preparation of $Ag^{II}(SO_3F)_2$ relied on the oxidation of various Ag-containing precursors with a very reactive sulfuryl peroxide for 168 h at 70 °C,[5] see for example Equation (1).

$$Ag + (SO_3F)_2 \rightarrow Ag(SO_3F)_2 \quad (1)$$

Here we have synthesized the title compound by using two novel reaction pathways. The first one, methathetic, was based on a ligand exchange between KSO_3F and $Ag(SbF_6)_2$[13] in anhydrous HF (aHF) according to Equation (2).

$$2KSO_3F_{(aHF)} + Ag(SbF_6)_{2(aHF)} \rightarrow Ag(SO_3F)_2\downarrow + 2KSbF_{6(aHF)} \quad (2)$$

Solid reagents [colourless KSO_3F, ocean blue $Ag(SbF_6)_2$] were mixed in a fluorinated ethylene propylene (FEP) reactor and aHF was condensed as a solid over the mixture at 77 K. The temperature was raised slowly above the melting point of aHF (–84 °C). As aHF melted, the droplets progressively dissolved reagents and a brown colour immediately appeared. The mixture was heated slowly to room temperature, and the $KSbF_6$ byproduct was washed away with new portions of aHF, thereby leaving insoluble brown residue of $Ag(SO_3F)_2$. The yield was close to 100% (based on the mass of washed-off $KSbF_6$). The product contained very few impurities as suggested by its Raman spectrum.

The second synthetic method was based on the reaction between AgF_2 and HSO_3F at room temperature or slightly above it [but less than 50 °C; Equation (3)].

$$AgF_2 + 2HSO_3F \rightarrow Ag(SO_3F)_2 + 2HF\uparrow \quad (3)$$

The reaction was, however, very slow and the conversion was not completed even after four months. Simultaneously, partial decomposition of brown $Ag(SO_3F)_2$ to black $Ag_3(SO_3F)_4$ could be noticed on the surface of the as-forming product, according to Equation (4).

$$4Ag(SO_3F)_2 + HSO_3F \rightarrow Ag_3(SO_3F)_4 + [AgSO_3F{\cdot}HSO_3F] + 3/2(SO_3F)_2\uparrow \quad (4)$$

If the reaction was stopped after four days, AgF_2 and $Ag(SO_3F)_2$ were the main crystalline phases with just a small amount of $Ag_3(SO_3F)_4$ impurity.

Very pure samples of $Ag(SO_3F)_2$, free of any paramagnetic impurities and used later for magnetic measurements, were obtained using the published reaction[5] [Equation (5)].

$$2AgSO_3F + (SO_3F)_2 \rightarrow 2Ag(SO_3F)_2 \quad (5)$$

$AgSO_3F$ precursor was obtained in a reaction between AgF (Sigma–Aldrich) and a large excess amount of HSO_3F (Sigma–Aldrich). Remnants of the acid were washed away with a mixture of CF_3COOH and $(CF_3CO)_2O$ in a volumetric ratio 1:3 followed by drying for 24 h under vacuum. The second substrate of the reaction [Equation (5)], $(SO_3F)_2$, was obtained from thermal decomposition of $Xe(SO_3F)_2$.[14]

Crystal Structure

$Ag(SO_3F)_2$ (Figure 1) grown from dark brown saturated HSO_3F as a product of the reaction [Equation (3)] formed long, beautiful needle-shaped single crystals, intergrown in the form of hedgehogs (Figure 2). The needles were extremely mechanically fragile and chemically reactive and they instantly decompose to colourless $Ag^{I}SO_3F$ if taken away from supernatant and placed inside a quartz capillary.

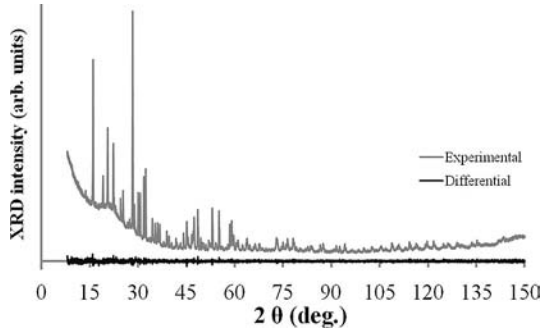

Figure 1. Powder XRD pattern of $Ag(SO_3F)_2$ obtained from Equation (3): experimental and differential curves are shown.

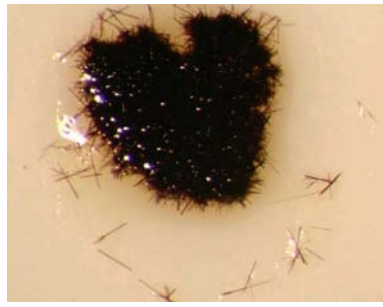

Figure 2. Long, needle-shaped dark brown single crystals of $Ag(SO_3F)_2$ grown from HSO_3F as a product of the reaction [Equation (3)] over several days, intergrown in the form of hedgehogs and of larger conglomerates.

The crystal structure of silver(II) fluorosulfate (Table 1, Figure 3) was therefore solved from the powder data. Re-

straints on geometry of fluorosulfuric anions were applied.[15] The sample used for refinement was obtained in a reaction [Equation (3)] that lasted for four days and it contained a considerable amount of AgF_2 [24.4(2) wt.-%] and some $Ag^{II}Ag^{I}_2(SO_3F)_4$ [9.1(2) wt.-%] (weight fractions were obtained from refinement). Only lattice vectors were refined for both minority phases [$Ag^{II}Ag^{I}_2(SO_3F)_4$[8] and AgF_2[16]].

Table 1. Crystallographic data for $Ag(SO_3F)_2$.

Space group	$P2_1/c$ (no.14)		
V [Å^3]	643.88(5)		
a [Å]	10.5130(4)		
b [Å]	7.7524(3)		
c [Å]	8.9366(4)		
β [°]	117.867(2)		
Z	4		
R_p	0.0244		
R_{wp}	0.0321		
$R_{(Bragg)}$	0.0276		
GOF	1.14		
R(Ag1–O) [Å]	2.053(18)	2.14(3)	2.61(2)
R(Ag2–O) [Å]	2.07(3)	2.154(19)	2.49(2)
R(S1–O) [Å]	1.48(3)	1.48(2)	1.417(18)
R(S2–O) [Å]	1.48(3)	1.48(3)	1.418(19)
R(S1–F1) [Å]	1.55(2)		
R(S2–F2) [Å]	1.55(2)		

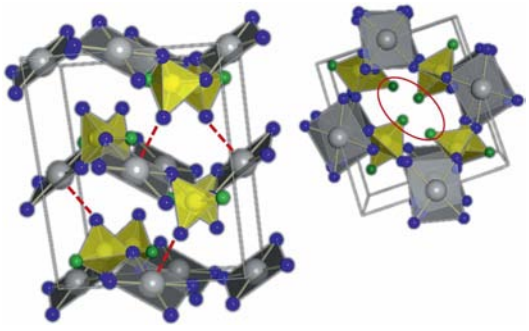

Figure 3. Crystal structure of $Ag(SO_3F)_2$. (left) The crystallographic unit cell; (right) view along the a axis emphasizing the presence of F channels. Grey balls: Ag, yellow balls: S, blue balls: O, green balls: F. Selected long (apical) Ag–O bonds are marked with red dotted lines.

The unit cell of $Ag(SO_3F)_2$ (Figure 3) contains two crystallographically independent Ag cations and two distinct types of fluorosulfuric anions. The Ag^{2+} cations are each coordinated by six oxygen atoms in the form of a distorted elongated octahedron; the four short Ag–O distances range between 2.053(18) and 2.154(19) Å, whereas the longer apical ones are between 2.49(2) and 2.61(2) Å. The short Ag–O separations are close to those found for other oxo compounds of divalent silver, such as $Ag^{II}(AgO_2)_2$ (2.052–2.086 Å)[4] or $Ag^{II}SO_4$ (2.094–2.198 Å).[7] Regretfully, the crystal structure of related $Cu(SO_3F)_2$ is not available for comparison.

The dimensionless Jahn–Teller distortion parameter, D, ranges from 1.245 for Ag1 to 1.179 for Ag2, and it is thus similar to the those observed for Ag^{II} in a fluoride environment.[17]

The short S=O bonds (ca. 1.418 Å) are localized at oxygen atoms to form long, more ionic bonds to Ag^{II} cations. The longer S–O bonds (ca. 1.48 Å) involve oxygen atoms that form short, more covalent bonds to Ag^{II}.

$Ag(SO_3F)_2$ forms puckered layers with the [AgS_2] sublattice, which is topologically very similar to the [AgF_2] sublattice of AgF_2.[16] The [$Ag(SO_3F)_2$] sheets are interconnected through the longest Ag–O bonds just like the [AgF_2] sheets are linked through the longest Ag–F bonds, thus enabling an intersheet magnetic exchange.[16] The Ag^{II} cations are linked within each sheet through OSO linkers from the SO_3F groups; direct Ag–O–Ag bridges are absent. As for several other fluorosulfates with modestly covalent metal–oxygen bonding, such as $Sn^{II}(SO_3F)_2$[18] or $Au^{III}(SO_3F)_3$,[19] fluorine is not bound to metal cation. Instead, terminal fluorine atoms stick towards one another while forming very narrow channels along the a crystallographic axis (Figure 3). The shortest F···F separation is 3.12(2) Å, which, compared to the doubled van der Waals radius of the F atom of 2.94 Å, leaves only 0.16 Å of free space. Thus, even the smallest hydrophobic atom, that of helium, cannot travel through the F channels of $Ag(SO_3F)_2$.

Vibrational Spectra

Structural complexity, low local C_1 symmetry of SO_3F moieties and the presence of two independent fluorosulfuric anions in the crystal structure are revealed in the rich-in-bands vibrational spectra of $Ag(SO_3F)_2$ (Figure 4).[20] The positions of the major IR bands are in fair agreement with those reported previously,[5] but we were able to identify more bands than in the previous study and provide Raman wavenumbers as well (Table 2).[5] It is clear that mutual exclusion principle applies, since the strongest IR bands are Raman-inactive and vice versa (recall, an inversion centre is present).

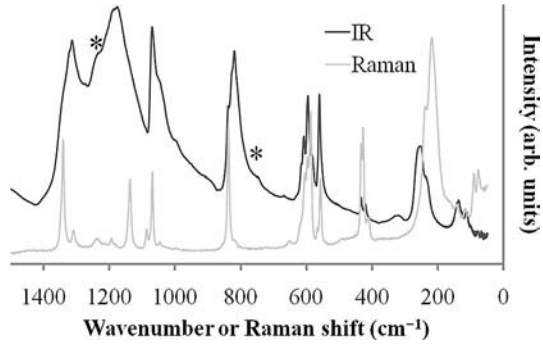

Figure 4. The IR and Raman spectra of $Ag(SO_3F)_2$. The asterisk (*) marks the strongest bands of the $Ag_3(SO_3F)_4$ impurity.

The wavenumbers of characteristic IR-active S–O stretching and O–S–O deformation modes reconfirms presence of covalently bound tridentate fluorosulfuric anions.[21] Specific are:[22]

Table 2. IR and Raman bands of $Ag(SO_3F)_2$ with intensities and assignment together with the theoretical DFT values (LDA; for GGA see the Supporting Information).[a]

IR (ref.[5])	IR	Raman	DFT (LDA)	Assignment
1320 (s, br.)	1320 (w, sh)	1340 (s)		SO_3 str.
	1313 (s)	1309 (w)		
1185 (vs, br.)	1188 (s, sh)	1239 (vw)		
	1176 (vs, br.)	1194 (vw)	1282–1026	
		1134 (s)		
1070 (s, br.)	1070 (s)	1086 (w)		
	1046 (m, sh)	1069 (s)		
	838 (w)	838 (s)	813–773	SF str.
	826 (w, sh)	819 (vw)		
820 (ms)	820 (s)			
	615 (w, sh)		587–522	SO_3F def.
	608 (m)	604 (w)		
	595 (m)	598 (s)		
	560 (m)	587 (s)		
		558 (s)		
	434 (w)	434 (s)	419–392	SO_3F rock.
	421 (w)	428 (s)		
		415 (vw)		
		410 (w)		
	255 (s)		279–34	AgO str. and lattice
	236 (s)	238 (vs)		
		219 (vs)		
	138 (w)	141 (w)		
	114 (w)	118 (w)		
		91 (m)		
		78 (w)		

[a] v: very, s: strong, m: medium, w: weak, br.: broad, sh: shoulder, str = stretching, def = deformation, rock = rocking.

(i) a strong band above 1100 cm^{-1} that corresponds to S–O stretching is split into three centred at 1313, 1180 and around 1170 cm^{-1}, thus making this part of spectrum similar to that of $Cu(SO_3F)_2$,[22,23]
(ii) the band above 1300 cm^{-1} that corresponds to S=O stretching points to the presence of oxygen that is bound more weakly to Ag^{II} but more strongly to S,
(iii) the O–S–O deformation modes are stiffened with ν_5 above 600 cm^{-1} and ν_3 above 560 cm^{-1},
(iv) the S–F stretching frequencies are well above 800 cm^{-1}, which is consistent with the fact that all F atoms are terminal and thus indirectly suggests a more covalent Ag–O bonding. The absorption band is narrow and intense, in contrast to those observed for ionic fluorosulfates (broad and weak).[24]

The Raman spectrum (Figure 4) is also rich in bands due to the presence of four formula units (FUs) inside the crystallographic unit cell and concomitant Davidoff splitting and/or Fermi resonances (coupling of different tones, overtones or combination modes).

Chemical Reactivity

In most reactions we have attempted, $Ag(SO_3F)_2$ behaves like a moderately strong Lewis acid and a strong oxidizer. For example, it has been known that $Ag(SO_3F)_2$ may form pseudoternary salts with fluorosulfates of Ag^I and K^I.[5] Our own results confirmed the existence of these salts;[11] however, we note that they cannot be formed in a direct reaction between the corresponding pseudobinary fluorosulfates, see for example Equation (6).

$$Ag(SO_3F)_2 + 2Ag(SO_3F) \rightarrow Ag_3(SO_3F)_4 \quad (6)$$

This is due to a lack of thermal stability of the $Ag(SO_3F)_2$ precursor (see next section). Even if the solid–solid reaction is conducted for two weeks at a temperature as low as 80 °C, complete decomposition takes place of dark brown $Ag(SO_3F)_2$ to colourless Ag^I-containing products.

It is conceivable that, as with AgF_2, $Ag(SO_3F)_2$ might behave like a weak Lewis base towards stronger Lewis acids, for example, HSO_3CF_3 or $HSbF_6$. Indeed, displacement reactions using these acids [see Equations (7) and (8)] are very fast and efficient and they result in, respectively, insoluble brown $Ag(SO_3CF_3)_2$[6] and an ocean-blue-coloured solution of $Ag(SbF_6)_2$ in an excess amount of aHF (together with colourless Ag^I-containing residues).

$$Ag(SO_3F)_2 + 2HSO_3CF_3 \rightarrow Ag(SO_3CF_3)_2 + 2HSO_3F \quad (7)$$

$$Ag(SO_3F)_2 + 2HSbF_6 \rightarrow Ag(SbF_6)_2 + 2HSO_3F \quad (8)$$

Reactions between $Ag(SO_3F)_2$ and HSO_3CF_3 or $HSbF_6$ could not be stopped at the intermediate stage of $[Ag(SO_3F)^+]\mathbf{L}^-$ salts (in which $\mathbf{L} = SO_3CF_3$, SbF_6). In view of lack of thermal and thermodynamic stability of $Ag(SO_3F)_2$ (see next section), it is conceivable that compounds that contain an even more acidic and coordinatively less saturated $Ag(SO_3F)^+$ moiety would be even more thermally unstable than $Ag(SO_3F)_2$, and they should be sought at low temperatures only.

$Ag(SO_3F)_2$ is not soluble in any common inorganic or organic solvent. Similarly to AgF_2[25] it vigorously reacts with water and even with anhydrous sulfuric or nitric acid. $Ag(SO_3F)_2$ is decomposed by dimethylformamide, *N*-methylformamide, tetrahydrofuran, nitromethane (with evolution of unidentified colourless gas[26]) and perfluoropyridine. In contrast to AgF_2,[27] $Ag(SO_3F)_2$ resists prolonged action of hexane, cyclohexane and sulfolane (tetrahydrothiophene 1,1-dioxide) and unlike AgF_2 it is decomposed by CCl_4 to AgCl within half an hour. Surprisingly, and similarly to AgF_2, $Ag(SO_3F)_2$ is inert toward *tert*-butyl alcohol and perfluoro-*tert*-butyl alcohol (despite the fact that peroxides of these alcohols are known).

$Ag(SO_3F)_2$ easily oxidizes I_2 and Br_2 to yield the corresponding silver(I) halides. Reaction with Ce^{III} sulfate in HSO_3F is much slower but after one week partial conversion to characteristic orange-coloured Ce^{IV} complexes can be noticed. $Ag(SO_3F)_2$ is reduced within 3 h by solution of nitrosobenzene in hexane. None of the redox reactions studied may be stopped at intermediate stage that corresponds to a mixed-valence Ag^I/Ag^{II} fluorosulfate; full reduction of Ag^{II} to Ag^I is always observed.

Thermal Analysis

Leung and Aubke[5] reported the temperature of the thermal decomposition of Ag^{II} fluorosulfate as 210 °C but they did not specify chemical nature of the products of decomposition. Our own thermogravimetric analysis (TGA)/differential scanning calorimetry (DSC) measurements (Figure 5) suggest, however, that $Ag(SO_3F)_2$ slowly decomposes thermally even at 30 °C (faster at $T > 120$ °C), thus it is thermally less stable than previously reported. Decomposition leads to the evolution of yellowish fumes of ($SO_3F^{\cdot}$) radical and to Ag^{I} fluorosulfate according to Equations (9) and (10) (theoretical values of mass loss related to initial substrate are given in brackets).

$$Ag(SO_3F)_2 \rightarrow AgSO_3F + 1/2(SO_3F)_2\uparrow \ (-32.4\ \text{wt.-\%}) \quad (9)$$

$$(SO_3F)_2 \rightarrow 2SO_3F\uparrow \quad (10)$$

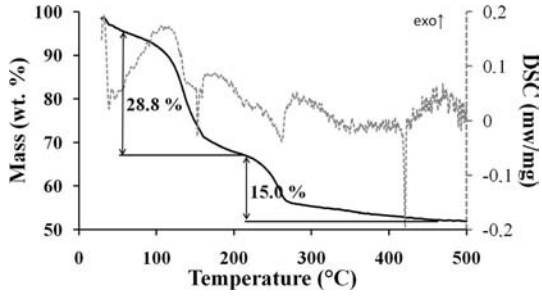

Figure 5. The TGA/DSC profiles of $Ag(SO_3F)_2$ measured in Ar flow at 5 K min^{-1} heating rate.

Decomposition does not stop at the $Ag_3(SO_3F)_4$ stage since this compound is equally unstable as $Ag(SO_3F)_2$[11] and it decomposes to $Ag^{I}SO_3F$. Further heating results in decomposition of $Ag^{I}SO_3F$ to Ag_2SO_4 with evolution of SO_2F_2 [Equation (11)], similarly to the process observed for $M(SO_3F)_2$ (M = Sr, Ba).[28]

$$2AgSO_3F \rightarrow Ag_2SO_4 + SO_2F_2\uparrow \ (-16.7\ \text{wt.-\%}) \quad (11)$$

Ag_2SO_4 is the ultimate product of thermal decomposition at 400 °C as confirmed by XRD and IR spectroscopy as well as the presence of the characteristic sharp endothermic peak of its phase transition at 425 °C in the DSC profile[29] (Figure 5).

The experimental values of mass loss for steps I and II of thermal decomposition (28.8 and 15.0%) agree fairly well with the theoretical values, assuming the occurrence of the reaction in Equation (9) at the first stage (32.4%) and of the reaction in Equation (11) at the second stage (16.7%). The fact that the observed mass losses are slightly smaller that the theoretical ones may be explained by spontaneous partial decomposition of unstable $Ag(SO_3F)_2$ specimen held for 1 h in a stream of Ar gas inside the TGA analyzer during conditioning of the sample.

The first step of thermal decomposition of $Ag(SO_3F)_2$ is more exothermic than the second one. In any case, the exothermicity of decomposition and evolution of gases (SO_3F, SO_2F_2) renders $Ag(SO_3F)_2$ thermodynamically unstable with respect to the products of decomposition. Decomposition is thus a spontaneous kinetically controlled process that occurs slowly even at room temperature. As a result, the surfaces of $Ag(SO_3F)_2$ crystals are often covered with black $Ag_3(SO_3F)_4$ salt. However, all attempts in the synthesis of $Ag_3(SO_3F)_4$ by means of controlled thermal decomposition of $Ag(SO_3F)_2$ at temperatures not exceeding 80 °C have failed.[11] $Ag^{I}(SO_3F)_2$ has been obtained in all cases.

Magnetic Properties and ESR Spectra

The presence of paramagnetic Ag^{2+} species gives rise to magnetic ordering phenomena in solids. The plot of the temperature dependence of magnetic susceptibility for silver(II) fluorosulfate in the 2–150 K temperature range is presented in Figure 6.

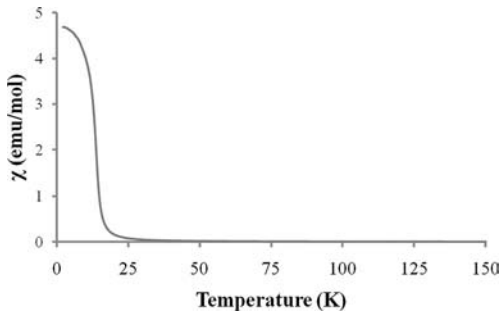

Figure 6. Magnetic susceptibility of $Ag(SO_3F)_2$ versus temperature measured in magnetic field of H = 1000 Oe.

$Ag(SO_3F)_2$ orders ferromagnetically with a Curie temperature, Θ, of 24.8 K estimated from a Curie–Weiss curve fit above 150 K. At first approximation the magnetic superexchange constant, J, for a 2D system such as $Ag(SO_3F)_2$ can be estimated from the mean-field approximation (i.e., Curie–Weiss law) and high-temperature series expansion by Baker et al.[30] as $\Theta/2$, thus yielding a J value of 1.0 meV.

The magnetic behaviour of $Ag(SO_3F)_2$ proves to be different from that of its antiferromagnetic (AFM) $AgSO_4$ sibling.[7] The magnetic ordering temperature is much lower than for $AgSO_4$ (here ordering is limited by thermal decomposition at ca. 400 K). These differences can be rationalized while taking into account different geometries of the magnetic superexchange pathways for both compounds (Figure 7). For $AgSO_4$ the superexchange goes through the double O–O bridge with both Ag–O–O and O–O–Ag angles close to 180°; the corresponding angles are much smaller for $Ag(SO_3F)_2$ and one of them is in fact closer to 90° (113–118°), hence its favour for the FM-type intrasheet exchange. In addition, the Ag–O distances between the layers are not very large (ca. 2.5 Å), whereas the angles of the intersheet Ag–O–O–Ag bridge deviate from 180° (154 and 98°), thus favouring an intersheet FM superexchange.

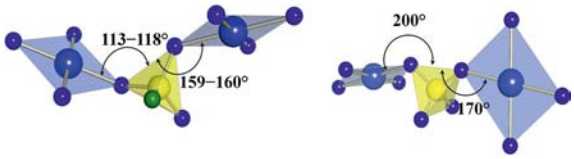

Figure 7. Geometries of the magnetic superexchange pathways (Ag···OO···Ag) for $Ag(SO_3F)_2$ (left) and related $AgSO_4$ (right).

The magnetic hysteresis measurement at 5 K (Figure 8) shows negligible hysteresis, hence $Ag(SO_3F)_2$ may be labelled as a soft ferromagnet. The saturated magnetic moment of 1.08 μ_B per FU agrees with the value of around 1 μ_B per FU expected for a $4d^9$ transition-metal cation.

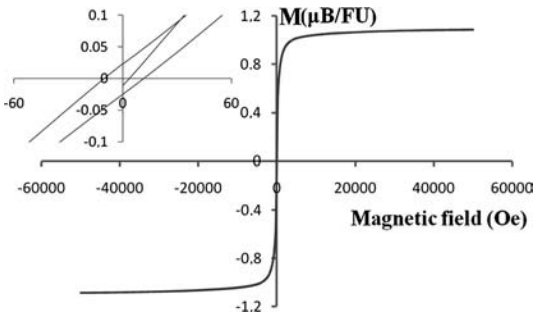

Figure 8. Magnetic hysteresis (M vs. H) of $Ag(SO_3F)_2$ at 5 K. The expanded region around (0,0) is shown in the inset.

The ESR spectra measured between 2.4 and 293 K are shown in Figure 9. The spectrum taken at room temperature shows only one broad line with g = 2.183; the g factor characteristic of $Ag(SO_3F)_2$ is different than the one of 2.119 measured for related $Ag^I_2Ag^{II}(SO_3F)_4$.[11] As the temperature is lowered the ESR band gets sharper, more intense and eventually splits in three. At 17.2 K, just below the temperature of ferromagnetic ordering (24.8 K), g factors have values of g_1 = 2.269, g_2 = 2.212 and g_3 = 2.136. The rhombic g tensor is of course not unexpected given the local 2+2+2 environment of Ag^{II}. However, at 2.4 K the ESR signal is split again with g factors of g_1 = 5.065, g_2 = 2.422 and g_3 = 1.248.

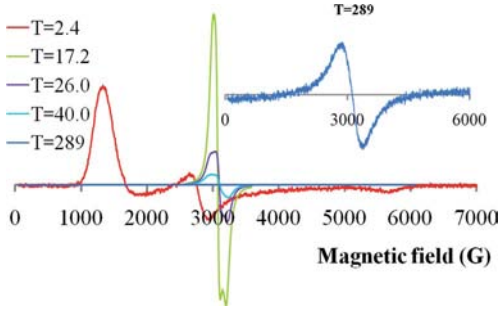

Figure 9. ESR spectra of $Ag(SO_3F)_2$ at five different temperatures [K].

Electronic Structure: A DFT Picture

To better understand the nature of magnetism and electronic structure of $Ag(SO_3F)_2$ we have carried out DFT calculations using local spin density approximation (LSDA) and Coulomb-corrected local spin density approximation (LSDA+U) methods. Two different projections of spin density within the crystallographic unit cell are shown in Figure 10. The electronic band structure and electronic density of states are shown in Figure 11. Magnetic moments on atoms are listed in Table 3.

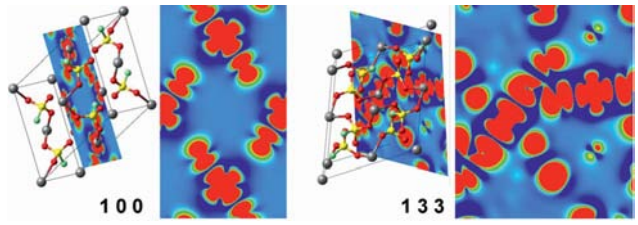

Figure 10. Two projections of spin density, ρ_{sp}, within the crystallographic unit cell as calculated for $Ag(SO_3F)_2$ at the LSDA+U level: –0.03 e Å^{-3} < ρ_{sp} < +0.66 e Å^{-3}. Projections emphasize the ferromagnetic character of both the intra- and intersheet superexchange.

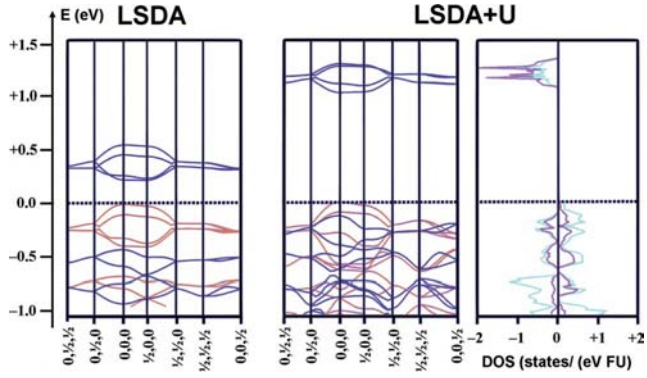

Figure 11. Electronic band structure at the LSDA level (left), at the LSDA+U level (middle) and electronic density of states (DOS) at the LSDA+U level (right) for $Ag(SO_3F)_2$. Spin majority channel: red, spin minority channel: dark blue. Colour code for partial DOS: summed contribution from all O atoms: light blue, both Ag atoms: violet.

Table 3. The magnetic moments on atoms as calculated for the FM ground state of $Ag(SO_3F)_2$ at the LSDA+U level.

Atom	μ [μ_B]	Atom	μ [μ_B]
Ag1	+0.51	O1, O1′	+0.08
Ag2	+0.50	O2, O2′	+0.09
S1, S2, F1, F2	0.00	O3, O3′	+0.02

The ferromagnetism of $Ag(SO_3F)_2$ arises from the magnetic superexchange of unpaired Ag(4d) electrons that reside at x^2–y^2 orbitals (localized within mutually inclined [AgO_4] squares) through the O–O bridges of the fluorosulfuric anions (Figure 10). The values of magnetic moments on Ag1/Ag2 atoms as obtained from the LSDA+U calculations are 0.50–0.51 μ_B, and thus larger than those calculated for ferrimagnetic $AgSO_4$ (±0.43–0.45 μ_B).[7] Simultaneously, the calculated values of magnetic moments on bridging O1/O2 atoms of 0.08–0.09 μ_B are slightly smaller than those calculated for respective atoms in $AgSO_4$

(±0.09–0.10 μ_B). These observations are in agreement with what might be anticipated from chemical character of SO_3F^- and SO_4^{2-} anions: the former one contains one highly electronegative fluorine atom and bears a single negative charge, in contrast to the latter anion, which contains only less electronegative oxygen atoms and bears a double negative charge. In consequence, sulfate dianion is more susceptible to oxidation by potent Ag^{II} oxidizer than is fluorosulfate anion, and thus chemical bonding between Ag^{II} and these oxa-anions somewhat differs; the ionic character is more pronounced for the $Ag^{II}\cdots OSO_2F^-$ bonding.

The more ionic character of the $Ag^{II}\cdots O$ bonding has some impact on the strength of magnetic superexchange. The intrasheet J estimated at the LSDA level of +1.1 meV per FU (thus +2.2 meV per each pair of interacting Ag^{II} centres[31]) is in very good agreement with the experimental value of +1.0 meV per FU. The value of J is thus much smaller (as far as absolute value is concerned) than the experimental value of –9.5 meV per pair of Ag^{II} cations for 1D ferrimagnetic $AgSO_4$.[7] This is only partially related to a slightly worse capability of SO_3F^- anions to transfer magnetic superexchange compared to SO_4^{2-} anions. The geometry of Ag–O–O–Ag bridges (with one O–O–Ag angle of 160° substantially departing from 90° and thus favouring AFM rather than FM superexchange) is to be blamed for that. Indeed, as we show in a separate contribution,[11] the potential of SO_3F^- anions to transfer magnetic superexchange is better revealed for antiferromagnetic $Ag_3(SO_3F)_4$ with its intrachain J value of –7.5 meV per pair of Ag^{II} cations due to the appropriate geometry of the bridging moieties.

LSDA calculations predict an unrealistically small value of the band gap at the Fermi level of 0.25 eV (Figure 11). The fact that the LSDA calculation does not converge to metallic solution indicates that supplementation of the LSDA method with the on-site electron repulsion U term is not necessary to stabilize the semiconducting magnetic state. However, the LSDA+U calculation leads to a larger direct band gap at Γ of 1.05 eV, which is consistent with the dark-brown colour of the compound (unfortunately, the experimental estimate of the band gap is currently unavailable). The value of 1.05 eV compares with 0.82 eV obtained previously at the same level of theory for black $AgSO_4$[7] which again indicates the more ionic character of $Ag(SO_3F)_2$. Inspection of the partial density of states (pDOS) for $Ag(SO_3F)_2$ (Figure 11) reveals that the states below the Fermi level are predominated by the contribution from oxygen atoms, whereas those above the Fermi level are predominated by the contribution from Ag, just as was calculated previously for $AgSO_4$.[7] $Ag(SO_3F)_2$ thus has a somewhat more pronounced charge-transfer insulator character than $AgSO_4$ (a Mott–Hubbard insulator).

Conclusions

In seeking to fill the gap in the data regarding synthesis, reactivity and characterization of rare oxa-derivatives of divalent silver, we have synthesized silver(II) fluorosulfate (first reported and briefly characterized in 1978[5]) and successfully solved its crystal structure from the powder X-ray data. Monoclinic $Ag(SO_3F)_2$ adopts a puckered-sheet structure related to that of AgF_2. The vibrational (IR and Raman) spectra confirm the presence of tridentate fluorosulfuric anions with a reduced local C_1 symmetry, covalently bound to a transition-metal cation. Two oxygen atoms are used for intrasheet bridging of the adjacent Ag^{II} cation, whereas the third one links the Ag^{II} cations from adjacent sheets. F atoms are terminal.

The presence of paramagnetic Ag^{II} cations is revealed by strong ESR absorption with g = 2.183 at room temperature. $Ag(SO_3F)_2$ is a soft ferromagnet with a Curie temperature of 24.8 K and magnetic superexchange constant of approximately 1.0 meV per FU. Density functional theory calculations show that the magnetic superexchange occurs through the O–O moiety of the Ag–O–S–O–Ag bridge while omitting the S atom, with J = +1.1 meV. Large magnetic moments reside on O atoms attached to Ag^{II} (close to 0.1 μ_B), thus facilitating spontaneous (exothermic) thermal decomposition of the title compound with emission of fluorosulfuryl radical ($SO_3F^{\cdot}$), which takes place (slowly) even at room temperature or in an acidic environment. $Ag(SO_3F)_2$ is a powerful oxidant that readily decomposes upon action of many common organic solvents, and it oxidizes elemental Br_2 (E^0 for Br_2/Br^I = +1.60 V vs. NHE) and even Ce^{III} (E^0 for Ce^{III}/Ce^{IV} = +1.76 V vs. NHE).

Experimental Section

General: All reactions were carried out under an Ar atmosphere (<0.1 ppm O_2 and <1 ppm H_2O) as provided by using a glovebox from MBraun or in a fluoropolymer vacuum line.

IR spectra were taken with a Vertex 80V vacuum spectrometer from Bruker. For the mid-IR region (500–7500 cm^{-1}) the powdered samples were placed on the surface of AgCl windows, whereas for far-IR (50–650 cm^{-1}) the samples were placed on polyethylene windows.

Raman spectra were recorded with a Horiba Jobin Yvon LabRam-HR Raman microspectrometer with a 632.8 nm He:Ne laser exciting beam. The power of the beam was reduced to a value of 0.17 mW to avoid photo- and thermal decomposition of the samples.

XRD powder patterns were obtained with a D8 discover diffractometer from Bruker equipped with a Cu cathode and a parallel beam setting provided by Göbel mirrors. The sample was loaded into a thin (0.3 mm diameter, 0.01 mm thick walls) quartz capillary from Hilgenberg. The structure solution was performed with Jana2006[32] coupled with Expo2004.[33] Topas 4.2 (Bruker AXS, 2009) was used to generate starting structural model for subsequent refinement. We employed Vesta to generate the structure visualizations.[34]

Further details on the crystal structure investigations may be obtained from the Fachinformationszentrum Karlsruhe, 76344 Eggenstein-Leopoldshafen, Germany (Fax: +49-7247-808-666; E-mail: crysdata@fiz-karlsruhe.de), on quoting the depository number CSD-422414.

Thermal analysis was performed with an STA 409PG TGA/DSC analyzer from Netzsch coupled with an Aëolos QMS 403C mass spectrometer (Netzsch) for evolved gas analysis. Samples (ca. 10 mg) were loaded into alumina crucibles. Heating rates of 1, 5 and 10 K min^{-1} were applied.

Magnetic measurements were conducted with a superconducting quantum interference device magnetometer MPMS-XL-5 from Quantum Design equipped with a 50 kOe magnet, and operating in the temperature range 2–300 K.

ESR spectra were taken with an ESP 300E spectrometer (frequency 9.5 GHz; X-band) from Bruker for samples sealed in Ar atmosphere inside a 4 mm thick quartz capillary.

Solid-state density functional theory (DFT) calculations were performed using the VASP code[35] with the projector-augmented wave method (PAW)[36] as implemented in the MedeA package. For the exchange-correlation part of the Hamiltonian, the local density approximation (LDA) in its local spin density approximation (LSDA) variant was applied, since we have noticed previously that LDA allows for much better reproduction than generalized gradient approximation (GGA) of the unit-cell parameters of related $AgSO_4$[37] (for the GGA-PBE and GGA-PW91 results, see the Supporting Information). During the full geometry optimization (cell and atomic parameters), the ionic relaxation was continued until the forces on individual atoms were less than 0.002 eV $Å^{-1}$. The electronic iterations convergence was set to 10^{-7} eV per atom by using the standard blocked Davidson algorithm and reciprocal space projection operators. The spacing between the points for the *k*-points mesh generation was around 0.5 $Å^{-1}$ (Monhorst pack of $5 \times 5 \times 5$). The valence electrons were described by plane waves with a kinetic energy cutoff of 600 eV, thereby yielding satisfactory convergence of total energy. Four different schemes of magnetic ordering were tested: one ferromagnetic: (i) further denoted as FM, with FM intrasheet and FM intersheet coupling, and three antiferromagnetic ones: (ii) AFM1 with AFM intrasheet and AFM intersheet coupling, (iii) AFM2 with AFM intrasheet and FM intersheet coupling, (iv) AFM3, with FM intrasheet and AFM intersheet coupling, as well as (v) a nonmagnetic cell. Total optimizations at the LSDA level for the above-mentioned unit cells have showed that the FM solution corresponds to a global energy minimum with all AFM solutions higher in total energy, and the nonmagnetic solution pushed above the FM one at as much as 35.4 meV per FU. For this reason, the unit cell of the FM solution optimized at the LSDA level was used for subsequent single-point calculations of energy of all magnetic ordering schemes in question.

The spin-polarized LSDA and LSDA+U single-point calculations were performed to derive the electronic and magnetic structure of $Ag(SO_3F)_2$ as well as the intrasheet magnetic superexchange constant, *J*. To mimic the strongly correlated nature of the 4d electrons of Ag and the interacting p electrons of the bridging "oxide anions" (within the superexchange Ag–O–O–Ag path), the value of the Coulomb integral U was set to 4 eV and Hund's exchange *J* to 1 eV for both of these ions; the respective values for S(3p) electrons were 2 and 1 eV, thus allowing direct comparison with results obtained earlier for $AgSO_4$.[7,37] The value of *J* was approximated by the difference of energy of FM and AFM2 configurations (which differ only in the spin flip within the sheets) as customary for 2D systems (this value was divided by the number of Ag^{II} cations per unit cell, $z = 4$). The appreciable difference in energy between the FM and AFM3 configurations (which differ only in sign of the intersheet magnetic coupling) of 0.3 meV per FU (LSDA+U) suggests that intersheet superexchange is quite strong for $Ag(SO_3F)_2$ (only one order of magnitude weaker than the intrasheet coupling), thus resulting in a quasi-3D magnetic character of this system at low temperatures.

Phonon frequencies at the centre of the Brillouin zone were calculated with VASP at the PAW LDA and PAW GGA-PBE level using atomic displacement of 0.002 Å with forces preoptimized down to 10^{-4} eV $Å^{-1}$ (for comparison of LDA phonon DOS and of experimental IR and Raman spectra, see the Supporting Information).

Supporting Information (see footnote on the first page of this article): More computational DFT results including the phonon density of states and assignment of vibrational bands are given.

Acknowledgments

This work is dedicated to Professor Felix Aubke in recognition of his significant contribution to chemistry of fluorosulfates. The project "Quest for Superconductivity in Crystal-Engineered Higher Fluorides of Silver" is operated within the Foundation for Polish Science "TEAM" Program cofinanced by the EU European Regional Development Fund. This work has been partly supported by the Slovenian Research Agency (ARRS) within the research program P1-0045 Inorganic Chemistry and Technology. Calculations have been performed on ICM supercomputers.

[1] W. Grochala, R. Hoffman, *Angew. Chem.* **2001**, *113*, 2816; *Angew. Chem. Int. Ed.* **2001**, *40*, 2742–2781.
[2] A. J. Bard, R. Parsons, J. Jordan, in: *Standard Potentials in Aqueous Solutions*, Marcel Dekker, IUPAC, New York, USA, **1985** (data accessed via www.webelements.com).
[3] W. Grochala, *Inorg. Chem. Commun.* **2008**, *11*, 155–158.
[4] B. Standke, M. Jansen, *Angew. Chem.* **1986**, *98*, 78; *Angew. Chem. Int. Ed. Engl.* **1986**, *25*, 77–78.
[5] F. Aubke, P. C. Leung, *Inorg. Chem.* **1978**, *17*, 1765–1772.
[6] P. C. Leung, K. C. Lee, F. Aubke, *Can. J. Chem.* **1979**, *57*, 326–329.
[7] P. J. Malinowski, M. Derzsi, B. Gaweł, W. Łasocha, Z. Jagličić, Z. Mazej, W. Grochala, *Angew. Chem.* **2010**, *122*, 1727; *Angew. Chem. Int. Ed.* **2010**, *49*, 1683–1683.
[8] J. L. Manson, K. H. Stone, H. I. Southerland, T. Lancaster, A. J. Steele, S. J. Blundell, F. L. Pratt, P. J. Baker, R. D. McDonald, P. Sengupta, J. Singleton, P. A. Goddard, C. Lee, M.-H. Whangbo, M. M. Warter, C. H. Mielke, P. W. Stephens, *J. Am. Chem. Soc.* **2009**, *131*, 4590–4591.
[9] F. Aubke, *J. Fluorine Chem.* **1995**, *71*, 199–200.
[10] P. Malinowski, Z. Mazej, W. Grochala, *Z. Anorg. Allg. Chem.* **2008**, *634*, 2608–2616.
[11] T. Michałowski, P. J. Malinowski, M. Derzsi, Z. Mazej, Z. Jagličić, P. J. Leszczyński, W. Grochala, *Eur. J. Inorg. Chem.* **2011**, 2508–2516, following paper.
[12] P. J. Malinowski, Z. Mazej, M. Derzsi, Z. Jagličić, J. Szydłowska, T. Gilewski, W. Grochala, *CrystEngComm*, manuscript submitted.
[13] D. Gantar, I. Leban, B. Frlec, J. H. Holloway, *J. Chem. Soc., Dalton Trans.* **1987**, 2379–2383.
[14] M. Wechsberg, P. A. Bulliner, F. O. Sladky, R. Mews, N. Bartlett, *Inorg. Chem.* **1972**, *11*, 3063–3070.
[15] Typical bond lengths and angles in the SO_3F^- anion were taken from published crystal structures of fluorosulfates with ionic and more covalent metal–oxygen bonds, such as $LiSO_3F$, $Sn(SO_3F)_2$, $Au(SO_3F)_3$, $FXe(SO_3F)$ and $(FXe)_2(SO_3F)(SbF_6)$. The angles were restrained at 113 (O–S–O) and 105° (O–S–F), whereas the distances at 1.42 Å (for S=O bonds, O is attached weakly to Ag at separation >2.4 Å), 1.48 Å (for S–O bonds, O is attached stronger to Ag at separation <2.2 Å) and 1.55 Å (for S–F bonds). The strength of the restraints allowed for a typical deviation of bond lengths of 0.005 Å and up to 5° for bond angles.

[16] A. Jesih, K. Lutar, B. Žemva, B. Bachmann, S. Becker, B. G. Müller, R. Hoppe, *Z. Anorg. Allg. Chem.* **1990**, *588*, 77–83.
[17] W. Grochala, *Phys. Status Solidi B* **2006**, *243*, R81–R83.
[18] D. C. Adams, T. Birchall, R. Faggiani, R. J. Gillespie, J. E. Vekris, *Can. J. Chem.* **1991**, *69*, 2122–2126.
[19] H. Willner, S. J. Rettig, J. Trotter, F. Aubke, *Can. J. Chem.* **1991**, *69*, 391–396.
[20] A small amount of impurities, notably $Ag_3(SO_3F)_4$, are certainly present in the samples that underwent spectroscopic analyses. $Ag(SO_3F)_2$ is thermally unstable and it partly decomposes even upon delicate grinding, which was necessary to obtain a good-quality IR spectrum and to load the capillary for Raman investigations. This spontaneous decomposition also occurs in the red laser beam used to excite the Raman spectra, so a low laser power (0.17 mW) was used to minimize this effect.
[21] G. A. Lawrence, *Chem. Rev.* **1986**, *86*, 17–33.
[22] C. S. Alleyne, K. O. Mailer, R. C. Thompson, *Can. J. Chem.* **1974**, *52*, 336–342.
[23] J. Goubeau, J. B. Milne, *Can. J. Chem.* **1967**, *45*, 2321–2326.
[24] S. P. Mellela, F. Aubke, *Can. J. Chem.* **1984**, *62*, 382–385.
[25] P. J. Malinowski, *MSc Thesis*, Faculty of Chemistry, University of Warsaw, **2008**.
[26] CH_3NO_2 is dehydrated by H_2SO_4 to give volatile HCNO; it might be that the fate of the reaction with $Ag(SO_3F)_2$ is similar.
[27] D. Grzybowska, *MSc Thesis*, Faculty of Chemistry, University of Warsaw, **2007**.
[28] E. L. Muetterties, D. D. Coffmann, *J. Am. Chem. Soc.* **1958**, *80*, 5914–5918.
[29] A. A. A. El-Rahmana, M. M. El-Desokyb, A. El-Wahab, A. El-Sharkawy, *J. Phys. Chem. Solids* **1999**, *60*, 119–127.
[30] G. A. Baker, H. E. Gilbert, J. Eve, G. S. Rushbrooke, *Phys. Rev.* **1967**, *164*, 800–817.
[31] The LSDA+U calculation leads to an overestimated value of *J* of +6.4 meV per FU.
[32] V. Petriček, M. Dušek, L. Palatinus, *Jana2006*, *The crystallographic computing system*, Institute of Physics, Praha, Czech Republic, **2006**.
[33] A. Altomare, R. Caliandro, M. Camalli, C. Cuocci, C. Giacovazzo, A. G. G. Moliterni, R. Rizzi, *J. Appl. Crystallogr.* **2004**, *37*, 1025–1028.
[34] K. Momma, F. Izumi, *J. Appl. Crystallogr.* **2008**, *41*, 653–658.
[35] G. Kresse, J. Furthmüller, *Phys. Rev. B* **1996**, *54*, 11169–11186.
[36] P. E. Blöch, *Phys. Rev. B* **1994**, *50*, 17953–17979.
[37] M. Derzsi, J. Stasiewicz, W. Grochala *J. Mol. Model.* **2011**, DOI: 10.1007/s00894-010-0950-y.

Received: January 22, 2011
Published Online: April 26, 2011

